Confirmation of Relativistic Energy-Momentum Relations using Compton Scattering

Syed Murtaza Husain
PHY 353L Modern Laboratory
Department of Physics
The University of Texas at Austin
Austin, TX 78712, USA

October 27, 2025

Abstract

In this experiment, we verify the relativistic relationship between energy and momentum for high-speed electrons produced via Compton scattering. Using a NaI(Tl) scintillation detector and multiple γ-ray sources, we measure the kinetic energy K and infer the momentum p of recoil electrons, allowing direct comparison of the nonrelativistic and relativistic energy–momentum relations. The measured data confirm that $E^2 = p^2c^2 + m^2c^4$ provides a better description than $K = p^2/2m$ for electrons with relativistic kinetic energies. We identify an unknown γ-emitter sample to be Cs-137 using Compton edge and photopeak energy determination. Using measured Compton edges and photopeak energies, we calculate the rest energy of the electron to be $m_ec^2 = 554.2 \pm 56.4$ keV, which is the accepted result within uncertainty. Finally, we apply an information-theory analysis of the Shannon entropy associated with the spectral complexity of increasing photopeak energies, and find a relation of the form $S = (0.792 \pm 0.03)\ln(E_\gamma) + (2.23 \pm 0.05)$, which is the expected logarithmic relation.

1 Introduction

1.1 Physics Motivation

One of the most well-known classical relations in physics is Newton's second law, which relates force, mass, and acceleration, is used ubiquitiously in mechanics and has been for centuries. In terms of momentum, Newton's second law can be restated to define force as the change in momentum over time. [9]. However, Albert Einstein introduced his famous energy-mass relation in 1905, which connected the total energy in a particle with its momentum, and overturned much of the classically held beliefs. Einstein's relationship is

$$E^2 = (pc)^2 + (mc^2)^2, \tag{1}$$

where p is the momentum, m is the rest mass and c is the speed of light [3]. At a very high velocity, $v \to c$, the kinetic energy. Writing $K = E - mc^2$ yields

$$K = \sqrt{(pc)^2 + (mc^2)^2} - mc^2 \tag{2}$$

while the classical (Newtonian) result,

$$K = \frac{p^2}{2m}, \tag{3}$$

is what we obtain when $p \ll mc$. An example of these results is shown in figure 1.

Although both relations are very similar for low-energy, low-speed motion, their predictions become very different once K is on the order of $m_ec^2 = 511\,\text{keV}$ for electrons. By testing equation 2 experimentally, we can confirm the validity of the relativistic model introduced by Einstein, and show how it diverges from the classical models. This will give us a greater understanding of how energy and momentum behave at very high speeds, as well as more insight into one of the most widely used and well-known laws of mechanics.

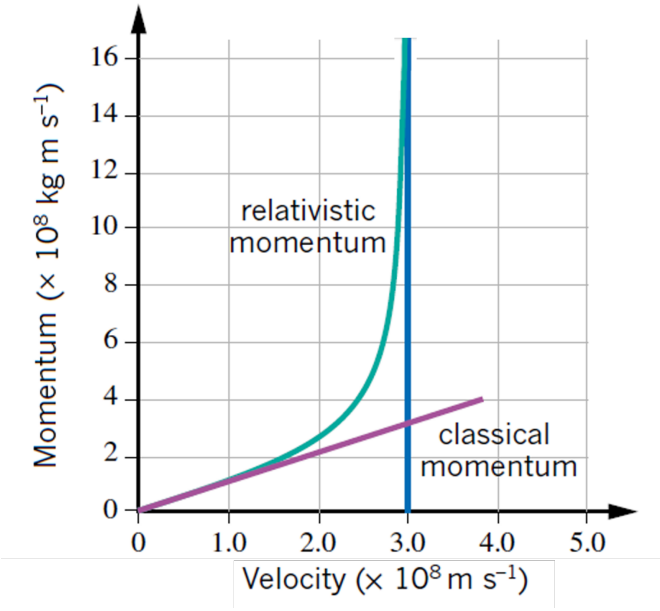

Figure 1: Example of divergence between relativistically and classically calculated momentums of particles as a funciton of velocity. When velocity is high, these results diverge. Image sourced from [8].

1.2 Theoretical Background

Beginning from the classical momentum expression (3), we expect a linear relationship for the kinetic energy of the electron, K, and its momentum, $p^2/2m_e$. Einstein's relativistic model instead predicts that K increases more slowly with p, following a nonlinear square-root dependence in Eq. (2). At small p the two curves are indistinguishable, but as $v \to c$, we should see the nonlinear, relativistic model more closely match our observations. To independently measure momentums of electrons without relying on either the classical or relativistic models, we utilize measurements of Compton scattering.

1.2.1 Compton Scattering and Recoil Momentum

Compton scattering occurs when γ-rays collide elastically with electrons which are previously at rest. This process was discovered by Arthur H. Compton in 1923 [1], and can be described as:

$$\gamma + e^- \to \gamma' + e^-$$

where the scattered photon will have lowere energy than it began with. The energy of the photon post-collision will be:

$$E'_\gamma = \frac{E_\gamma}{1 + \frac{E_\gamma}{m_e c^2}(1 - \cos\theta)} \tag{4}$$

Where θ is the angle of backscattering, and m_e is the mass of an electron. Conservation of energy and momentum gives the electron's recoil momentum

$$p = \frac{E_\gamma - E'_\gamma}{c} = \frac{E_\gamma}{c}\left(1 - \frac{1}{1 + \frac{2E_\gamma}{m_e c^2}}\right) \tag{5}$$

which reaches its maximum at $\theta = 180°$ backscattering [7]. This angle of maximum backscattering corresponds to the Compton edge observed in γ spectra from a scintillation detector. Since the incident photon energy E_γ is known from the source and the recoil electron's kinetic energy $K = E_\gamma - E'_\gamma$ is proportional to detector pulse height, equation 5 allows us to determine p totally experimentally.

1.2.2 Compton Edge Detection

To determine Compton edges from obtained spectra, we must find where the 180° backscattering angle occurs. With discrete spectra data, this is essentially equivalent to taking the derivative of the spectrum along the Compton continuum, and finding the point where the derivative is decreasing most sharply:

$$E_{\text{edge}} = \arg\min_E \left(\frac{dN}{dE}\right)$$

For discrete data points (E_i, N_i), this can be estimated numerically as

$$E_{\text{edge}} \approx E_i \text{ such that } \frac{N_{i+1} - N_{i-1}}{E_{i+1} - E_{i-1}}$$

$$= \min\left(\frac{N_{j+1} - N_{j-1}}{E_{j+1} - E_{j-1}}\right)$$

This position can be refined by fitting the local dropoff with an error function of the form

$$N(E) = A\left[1 - \text{erf}\left(\frac{E - E_{\text{edge}}}{\sqrt{2}\,\sigma}\right)\right] + B$$

where E_{edge} is the midpoint of the fitted drop and σ is the detector energy resolution [5].

1.3 Electron Rest Energy

Working backwards from the earlier equations, each measured photopeak energy E_γ and its corresponding Compton edge energy E_c can be used to determine the electron rest mass. Rearranging the Compton edge equation:

$$E_c = E_\gamma\left(1 - \frac{1}{1 + 2E_\gamma/m_e c^2}\right),$$

gives

$$m_e c^2 = \frac{2E_\gamma^2}{E_c(2E_\gamma - E_c)} \tag{6}$$

Using the measured values of E_γ and E_c for each emission source, $m_e c^2$ can be calculated and averaged to obtain an experimental estimate of the electron rest energy. The accepted value of $m_e \times c^2$ in eV is $511keV$.

[16]

1.4 Shannon Entropy

In information theory, the Shannon entropy quantifies the information content or uncertainty of a probability distribution. When applied to a gamma-ray energy spectrum, the entropy measures the spectral complexity of the detected photons. For a normalized intensity distribution p_i (where $p_i = I_i/\sum I_i$), the Shannon entropy is defined as

$$S = -\sum_i p_i \ln p_i.$$

Here p_i represents the probability of detecting a photon within energy bin i [18]. For an SRD, a spectrum with a sharp photopeak (such as at low photon energy) will show a smaller entropy, while a high energy gamma ray will create a broader spectrum with more Compton scattering, increasing the number of accessible states and by definition, the entropy.

As the photon energy E_γ increases, Compton interactions dominate and redistribute intensity across a wider range of channels [18]. The spectral entropy is expected to grow approximately as

$$S(E_\gamma) \propto \ln(E_\gamma),$$

This relationship can be compared directly to the measured spectral entropies extracted from each isotope's energy distribution.

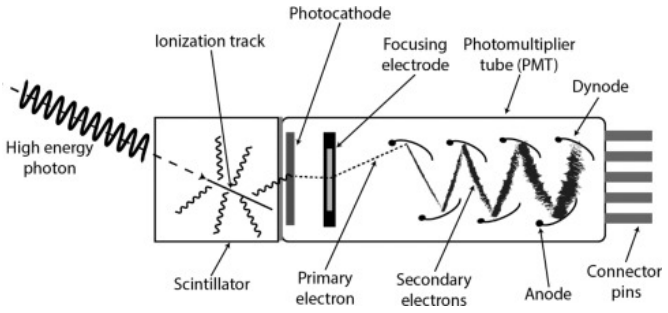

Figure 2: Diagram of scintillation radiation detector (SRD). High energy photons diffract into lower energy photons which induce a multiplied flow of electrons through the photomultiplier tube. Image sourced from [17].

1.5 Equipment Background

Understanding the equipment used in this experiment is vitally important to be able to quantify many of the effects we see.

1.5.1 Scintillation Radiation Detector

Scintillation radiation detectors (SRDs) are devices that consist of crystals which diffract high energy γ-rays into lower energy photons, which interact with a photocathode via the photoelectric effect. This causes electrons to be ejected into a photomultiplier tube (PMT) which has an array of dynodes and anodes that multiply electron output in a cascading fashion [2]. *ADD DIAGRAM. This tool will enable the collection of spectra for materials that emit gamma rays, and will allows us to view photopeaks and Compton edges. A diagram of an SRD is shown in figure 2

1.5.2 Signal Processing Equipment

In addition to the SRD, we require signal processing equipment to be able to make readings of the outputted analog signal. The piece of equipment directly connected to the output of the photomultiplier tube is the preamplifier, which has the purpose of forwarding the detected signal through the processing chain while minimizing the noise, or rather maximizing the signal-to-noise ratio of the reading [13].

We utilize a parasitic-capacitance preamplifier, which has a high input impedance of about 5 $M\Omega$ [14] and a capacitor in series with the resistor that creates a filter that reduces the impact of noise on the data. The preamplifier

is connected to a linear amplifier which boosts the signal by a configurable amount of gain.

1.5.3 Analog to Digital Devices

Finally, this analog signal is sent to a multi channel buffer (MCB) or multi channel analyzer (MCA). The MCA which consists of 1024 energy detection bins, while the MCB has a finer resolution of 8191 bins that will count the number of detections by photon energy and display them on the MAESTRO software as a large histogram. [10].

An MCB is a device that is very useful for nuclear spectroscopy applications because of its ability to turn the analog signals leaving the linear amplifier into a digital signal that can be recorded. The buffer temporarily stores data between the PMT and the computer's processor. Every time a detection signal is registered, the MCB will increment one of its 8191 bins which corresponds to the energy that the signal output [11].

The MCA has a very similar funciton with the distinction of having less bins which leads to coarser resolution. [12].

1.6 Our Approach

Through the use of a scintillation radiation detector, as well as signal processing equipment, we take several spectra of different radioactive elements that are γ-ray emitters, and find their Compton edges and photopeaks. We utilize both an Ortec multi-channel buffer and multi-channel analyzer to take separate readings and quantify the differences between the two devices. We use the Compton scattering model to determine the kinetic energies and momentums of electrons and then compare our results to both the classical and relativistic predictions to determine which model better describes our observations.

2 Experimental Setup

2.1 Apparatus

Our experimental apparatus includes an Ortec series 905 NaI(Tl) scintillation detector coupled to a photomultiplier tube (PMT), powered by a high-voltage supply at 0.7 kV, and connected to a chain of signal processing equipment: an Ortec series 113 scintillation preamplifier, an Ortec series 671 spectroscopy shaping amplifier, and an Ortec Aspec-927 dual multichannel buffer. Our preamplifier was set to 100 pF, and our shaping amplifier outputted 10 dB of gain. Several γ-ray sources were used to collect data, and are shown along with their known largest photopeak energies in table 1. Due to the detector resolution, manyy of these photopeaks and resulting Compton edges will be outside of our ability to detect. The data acquisition PC recorded spectra using ORTEC MAESTRO software. The complete setup is shown in figure 3.

Nuclide	E_γ (keV)	Intensity (%)
Ba-133	276.40	7.16
	302.85	18.33
	356.01	62.05
Co-57	122.06	85.60
	136.47	10.68
Co-60	1173.23	99.85
	1332.49	99.98
Cs-137	661.66	85.00
Mn-54	834.85	100.00
Na-22	511.00	179.80
	1274.54	99.94
Zn-65	1115.55	50.60
KCl	1460.83	10.67

Table 1: Largest photopeak energies for sources given in the lab materials. We expect to find these values when calibrating for energy and checking photopeak values in our data [6].

2.2 Calibration

2.2.1 MCB Energy Calibration

To begin the MCB energy calibration process, we recorded a spectra of a source for which we already know the photopeak values. This source was Na-22, which has 511 keV and 1275 keV lines. Having the spectra and known energies of the photopeaks allows us to create a mapping bewteen MCB channel and energies. By creating this mapping and ensuring that all of our readings are taken with the same amplifier and preamplifier settings, we can determine the energies for each bin of counts across the spectrum. The energy scale is determined from the linear equation

$$E = a + b\,C \tag{7}$$

where C is the channel number, b the energy per channel, and a the offset. Calibration uncertainty was dom-

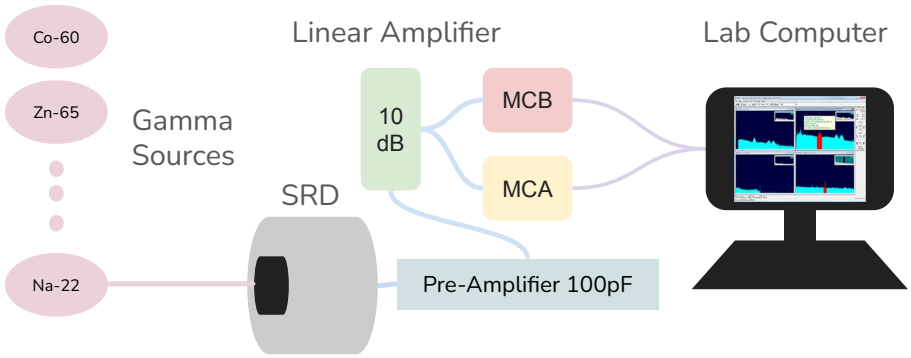

Figure 3: Diagram of experimental setup. Multiple different γ-emission sources are measured using the SRD, which has signal driven through processing equipment and then is recorded through either an MCB or MCA connected to the lab computer.

inated by channel resolution and statistical spread in counts [12].

After fitting to the MCB recorded Na-22 spectrum, we find fit parameters that are shown in figure 4.

2.2.2 MCA Energy Calibration

Similarly to the procedure for the MCB, we can use the same linear fit equation 7 to obtain an energy mapping for energy from bin using the Na-22 sample. This is shown in fig 5.The MCA has a more sensitive response than the MCB, meaning the count rate is higher even for the same live time [10].

The propagation of error in the calibration process is discussed in section 2.3.

2.2.3 Dark Spectrum

To reduce the impact of room noise on our SRD data, we take dark spectra using both the MCA and MCB for later calibration, in which we will subtract our observed data by the dark spectra. For readings that have different lengths of time than the recorded dark spectra, we can scale the dark spectra by the time difference to still utilize our dark subtraction method. Both of the dark spectra taken over 130 seconds of live time are shown in figure 6.

Using our calibration equation for the MCB 4b, we find that the dark spectra peaks appear at 19.31 keV and 650.37keV. For the MCA, using equation 5b, we find that the peaks appear at 25.98 keV and 649.44 keV. Uncertainties for these quantities are omitted because of their role as subtractive features that serve to correct errors in actual measurements.

2.3 Measurement Error Analysis

A significant amount of measurement error comes from the room light and dark spectra of our SRD. This was discussed in section 2.2.3. Another consideration is the discrete nature of the MCB bins limiting our precision in determining the energies within each bin of counts. Each MCA bin, for a large amount of counts, has an approximately normal distribution of counts across energy within each bin. Then the uncertainty within a bin is $\sigma_{Nx_i} = \sqrt{N(x_I)}$. The total uncertainty is then $\sigma_{x_{peak}} = \frac{\sigma_{cb}}{\sqrt{N_{peak}}}$, where $\sigma_{\bar{x}}$ is the standard deviation of the Gaussian fit to the peak, and N_{peak} is the total number of counts under the peak.

Knowing this, the uncertainty propagates from the calibration equation 7 to become $\sigma_E = a\sigma_{\bar{x}}$ where σ_E is the uncertainty in the energy of a peak [15].

When using this data to calculate the Compton edge, the error from E_γ will propagate to E_c. By standard propagation of uncertainty:

$$\sigma_{E_c} = \left|\frac{dE_c}{dE_\gamma}\right| \sigma_{E_\gamma}, \quad \text{where} \quad \frac{dE_c}{dE_\gamma} = 1 - \frac{1}{\left(1 + \frac{2E_\gamma}{m_e c^2}\right)^2}$$

So the final uncertainty in Compton edge energy is:

$$\sigma_{E_c} = \left(1 - \frac{1}{\left(1 + \frac{2E_\gamma}{m_e c^2}\right)^2}\right) \sigma_{E_\gamma} \tag{8}$$

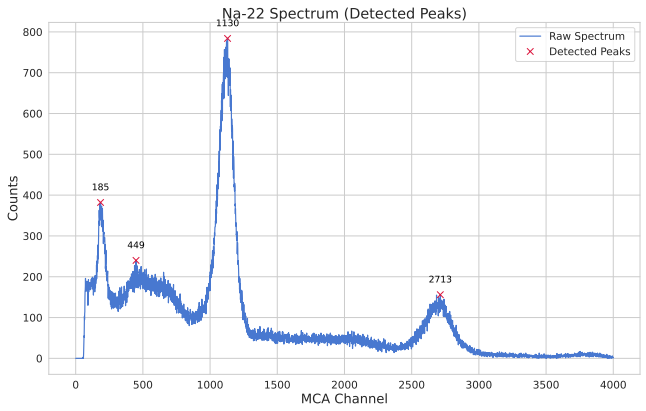

(a) Detected photopeaks for a spectrum of Na-22 taking using the MCB with 130s of live time. Detected peaks were matched to known energies for calibration purposes and subtracted from the dark spectrum.

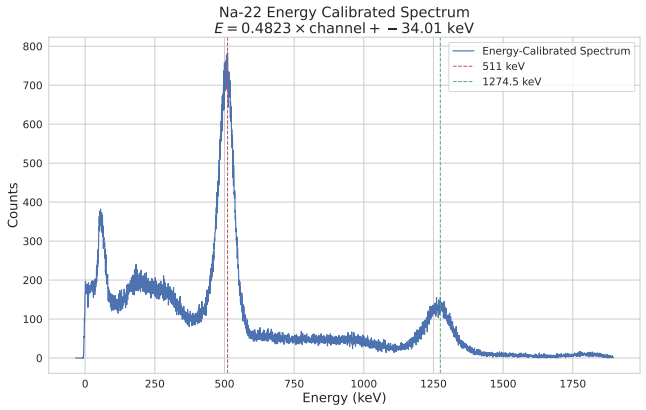

(b) Linear fit for MCB calibration energies given in equation 7 by matching known peaks to observed bins. Final fit was determined to be $E = 0.4823C - 34.01\ keV$ where C is MCB channel.

Figure 4: MCB Energy calibration with Na-22.

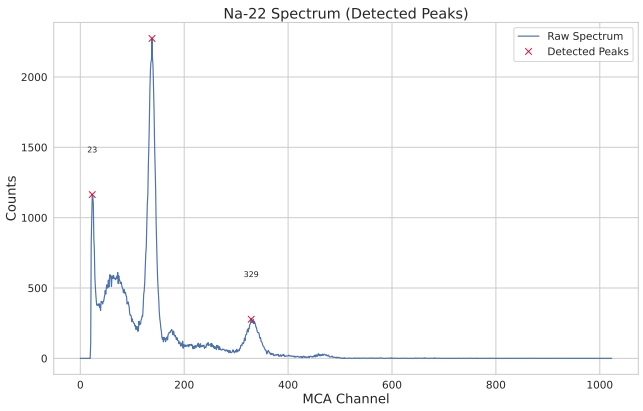

(a) Detected photopeaks for a spectrum of Na-22 taking using the MCA with 130s of live time. Compared to the MCB dark spectrum, counts were much higher, suggesting the MCA has a larger impact from noise.

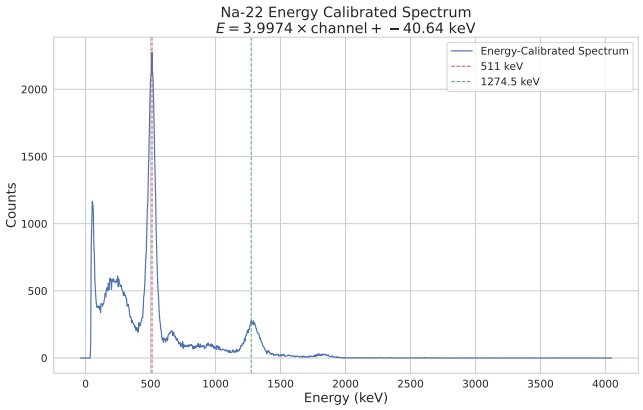

(b) Linear fit for MCA calibration energies given in equation 7 by matching known peaks to observed bins. Final fit was determined to be $E = 3.9974C - 40.64\ keV$ where C is MCB channel.

Figure 5: MCA Energy calibration with Na-22.

2.4 Data Collection

After undergoing calibration and equipment setup, we entered a lengthy data collection process. The full list of measurements taken is shown in table 2. Data collection ranged from 130 - 400 seconds of live time with the notable exception of KCl, which was recorded over the span of about 3.7 days.

3 Data Analysis and Results

3.1 Compton Edge Detection

Utilizing the logic outlined in section 1.5.1, we can numerically approximate the derivatice of the spectrum, $\frac{dN}{dE}$ and find Compton edges for each spectrum. To accomplish this, we first must restrict the region that we find the derivative of, to avoid finding the steepes photopeak's dropoff as the region of steepest decrease. This is dones by first finding the peaks in each spectrum and ranking them by prominence, and then manually creating a range that excludes clear photopeaks and includes the regions in which we can observe the Compton edge [7]. The results of this averaged across all of our spectra files are shown in table 3 and some example spectra of individual matches are shown in figure 7. For spectra such as Co-60 with two prominent peaks, this procedure can be run twice and the derivative can be calculated within the region before each peak.

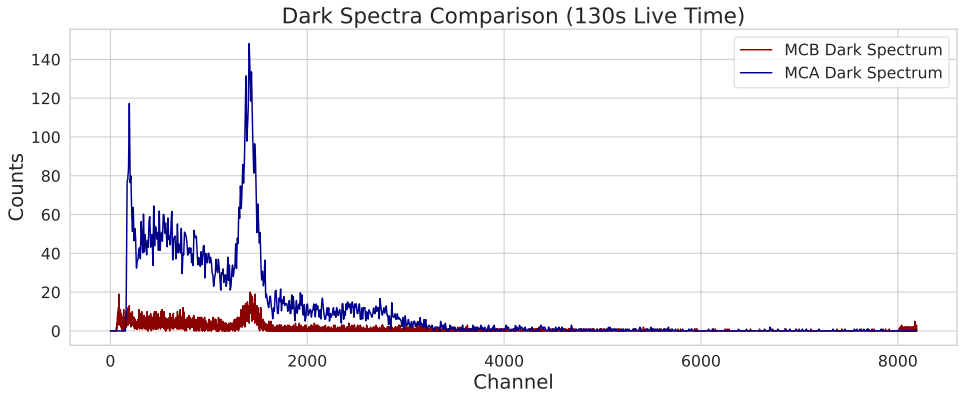

Figure 6: Dark spectra of SRD with lead insert, taken on both MCA and MCB. Readings were taken for 130s of live time and will be used for later dark subtraction during spectra data processing. .

Table 2: Nuclides measured during the experiment, along with SRD live time and detector type. Dark spectra for both MCA and MCB were also recorded. Uncertainty in live time is $\pm 0.5\,\mathrm{s}$.

Detector	**Nuclide**	**Live Time (s)**
MCA	Ba-133	130
MCB	Ba-133	130, 300, 400
MCA	Co-57	131
MCB	Co-57	130, 300, 400
MCA	Co-60	130, 210
MCB	Co-60	130, 300, 440
MCA	Cs-137	130
MCB	Cs-137	130, 300, 400
MCA	KCl	319682
MCA	Mn-54	130
MCB	Mn-54	130, 300, 400
MCA	Na-22	130, 150
MCB	Na-22	130, 400
MCA	Zn-65	136
MCB	Zn-65	130, 300, 400
MCA	Unknown	130
MCB	Unknown	130, 300, 400

3.2 Momentum Determination

With peaks and Compton edges known, it is now possible to calculate the momenta and energies of the electrons using the recoil momentum equation 5. For each nuclide, we can calculate this and determine whether or not the classical or relativistic model provides a better prediction of the momentum. The results we obtain overwhelmingly show that the relativistic fit better describes our observations. This is shown in figure 8. We obtain almost negligible residuals for the relativstic predictions, on the order of 10^{-32}, while there is significant disagreement between the classical predictions and measured results.

Nuclide	E_γ (keV)	E_c (keV)
Ba-133	356.5 ± 1.8	172.4 ± 1.7
Na-22	511.5 ± 2.6	347.5 ± 2.4
Co-60a	1173.0 ± 5.9	1000.0 ± 5.0
Co-60b	1330.2 ± 6.7	1194.4 ± 5.6
Co-57	136.0 ± 0.7	70.2 ± 0.7
Cs-137	665.3 ± 3.3	478.2 ± 3.0
Mn-54	841.1 ± 4.2	648.4 ± 3.7
Zn-65	1140.0 ± 5.7	860.7 ± 4.8
KCl	1501.2 ± 7.5	1216.1 ± 6.2

Table 3: Detected photopeak energies (E_γ) and calculated Compton edge energies (E_c) with propagated uncertainties for each nuclide. Co-60 includes both prominent γ lines.

3.3 Unknown Sample Identification

Using our measurements of the unknown sample, we devise a method to identify it using measured photopeak values and calculated Compton edge values. By matching these values to a known spectra database such as the Idaho National Laboratory database of gamma ray spectroscopy [6], we can determine what the sample is.

After matching these readings and calculations to the INL database as well as the other sources in our experiment kit, we determine that this source is Cs-137.

3.4 Electron Rest Energy Calculation

According to the theory outlined in section 1.3, we can experimentally estimate the rest mass of an electron. This process involved calculating rest mass using equation 6 and taking the average across the different spectra we

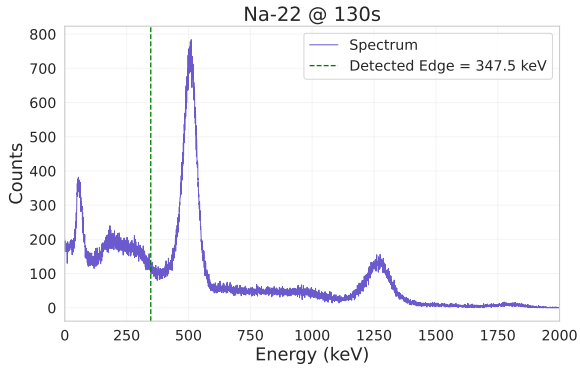

(a) Spectrum and compton edge detection for Na-22 for 130 seconds of live time.

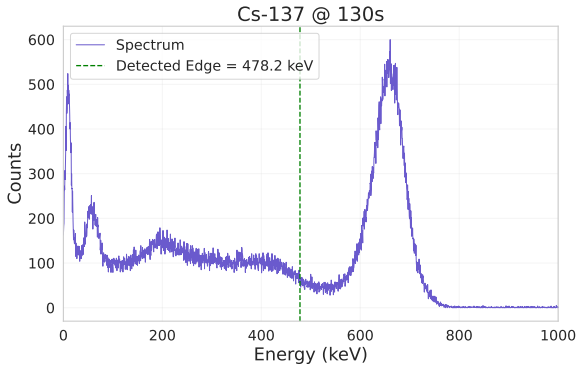

(b) Spectrum and compton edge detection for Cs-137 for 130 seconds of live time.

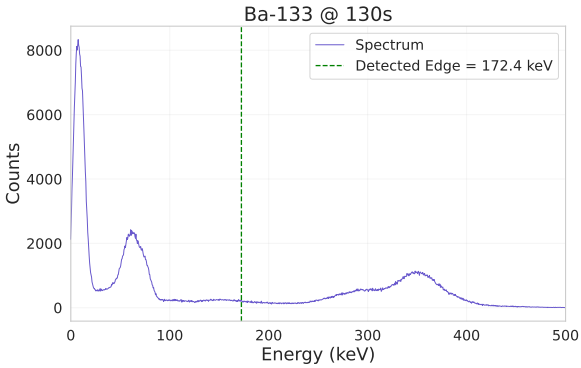

(c) Spectrum and compton edge detection for Ba-133 for 130 seconds of live time.

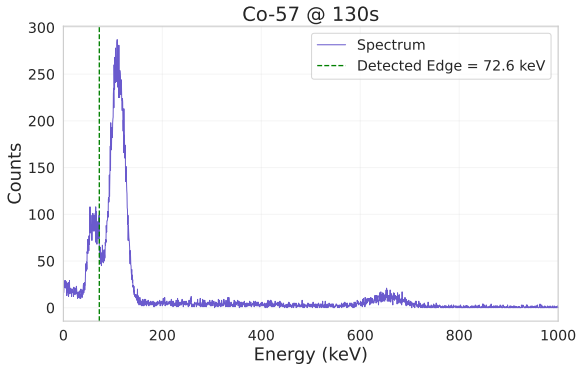

(d) Spectrum and compton edge detection for Co-57 for 130 seconds of live time.

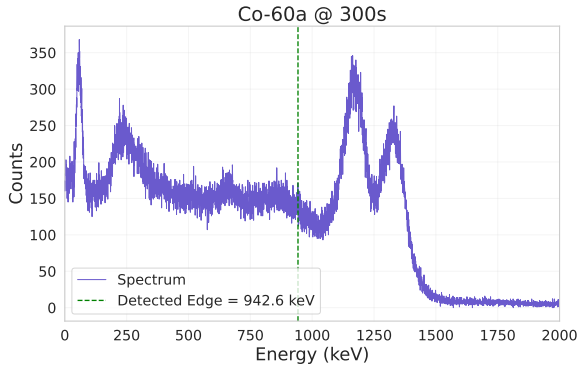

(e) Spectrum and compton edge detection for Co-60's first line for 300 seconds of live time.

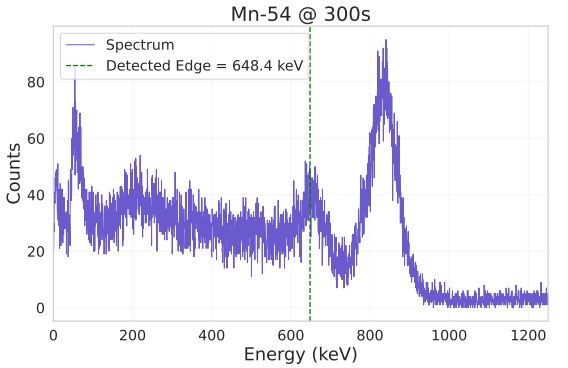

(f) Spectrum and compton edge detection for Mn-54 for 300 seconds of live time.

Figure 7: Compton edge detections for an example subset of detected spectra. The detection method involves detecting all peaks, classifying them by prominence, and then looking at the region before the peak to detect a Compton edge by calculating which area has the steepest negative derivative. Peaks to be observed were hardcoded after being detected via signal prominence detection.

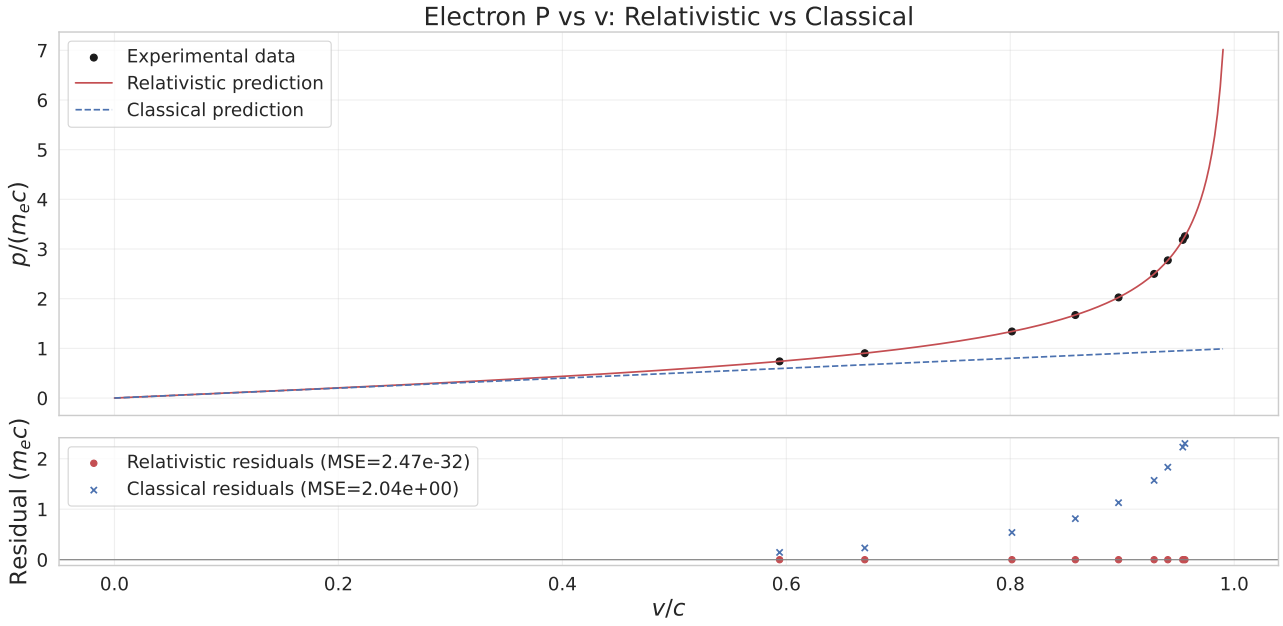

Figure 8: Classical vs relativistic predictions for measured data with residuals. Results show very high agreement with the relativstic model and exceedingly low residuals, while the classical model can be seen to diverge from measured data.

recorded. Our error for this process was the standard deviation of the calculated rest masses we obtained, which was unfortunately quite high. This could be due to detector response, different numbers of counts across samples due to their age and intrinsic emissivity, and other signal noise. Our calculation is shown in figure 10. The final result we obtain is $m_e c^2 = 554.2 \pm 56.4 keV$.

3.5 Shannon Entropy Analysis

The Shannon entropy was computed for each spectrum according to the theory outlined in section 1.4. Each SRD detection file was treated as a discrete probability distribution p_i and the resulting entropies were plotted against the corresponding photon energies for all available sources.

A clear increasing trend is observed where we see that lower energy sources such as Co-57 and Ba-133 have relatively low entropy ($S \approx 6.2$), which is consistent with narrow photopeaks and minimal Compton broadening, while high energy sources such as Co-60 and KCl reach values around $S \approx 8.0$, reflecting a much wider spread of scattered photon energies.

A logarithmic fit, which we expected to capture the behavior of the entropy, finds the following best fit parameters:

$$S = (0.792 \pm 0.03)\ln(E_\gamma) + (2.23 \pm 0.05)$$

4 Summary and Conclusions

4.1 Measured vs Known Compton Edges

This shows very good agreement with theoretical values, with the nuclides with the largest differences either being very energetic like Co-60, which falls in the regime where our detector is less reliable, or have very low count rates such as Zn-65, meaning noise in the data has a large impact on the measurement.

4.2 Shannon Entropy Discussion

The fitted slope in figure 11 agrees in magnitude with the empirically expected trend (dashed curve), suggesting that the detector's information content scales nearly logarithmically with the photon energy.

Physically, this indicates that as the gamma-ray energy increases, the NaI(Tl) detector records a spectrum containing more possible outcomes (more spread in energy deposition), and has a higher information entropy. This

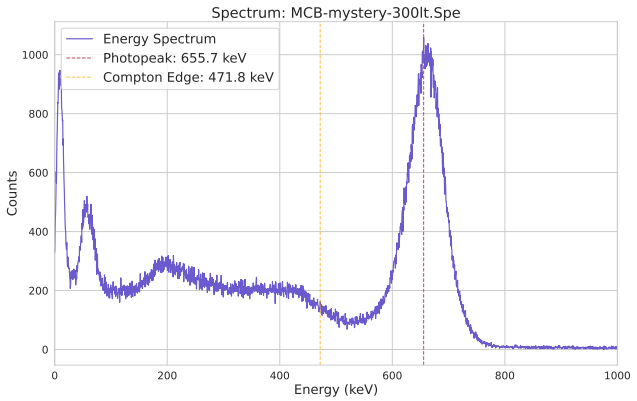

(a) Detected peak and calculated Compton edge for mystery sample over 300 seconds of detector live time. Data was taken using the MCB.

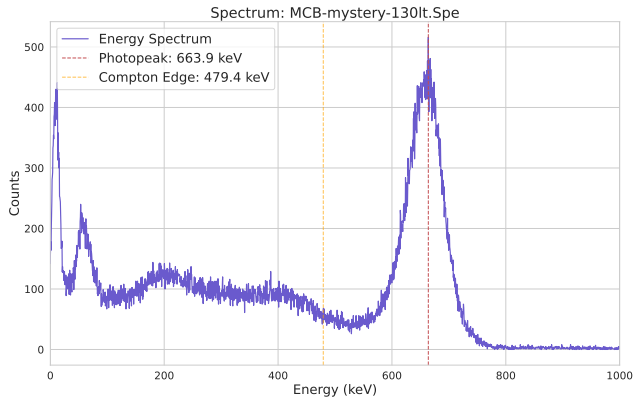

(b) Detected peak and calculated Compton edge for mystery sample over 130 seconds of detector live time. Data was taken using the MCB.

Figure 9: Two MCB recorded spectra of the unknown γ-emitter source with different detector live times. The spectra looks extremely similar to that of Cs-137, which is shown in figure 7b.

Table 4: Comparison of measured and reference photopeak energies (E_γ) and Compton edge energies (E_c). Theoretical E_c values are computed using $E_c = E_\gamma \left(1 - \frac{1}{1+\frac{2E_\gamma}{511}}\right)$. Photopeak data was taken from the IAEA γ-ray standard database [4].

Nuclide	$E_{\gamma,\text{ref}}$ (keV)	$E_{\gamma,\text{meas}}$ (keV)	$E_{c,\text{theor}}$ (keV)	$E_{c,\text{meas}}$ (keV)	$\Delta E_c = E_{c,\text{meas}} - E_{c,\text{theor}}$ (keV)
Ba-133	356.0	356.5 ± 1.8	162.0	172.4 ± 1.7	$+10.4 \pm 1.7$
Na-22	511.0	511.5 ± 2.6	340.67	347.5 ± 2.4	$+6.8 \pm 2.4$
Co-60a	1173.2	1173.0 ± 5.9	963.39	1000.0 ± 5.0	$+36.6 \pm 5.0$
Co-60b	1332.5	1330.2 ± 6.7	1118.11	1194.4 ± 5.6	$+76.3 \pm 5.6$
Co-57	136.5	136.0 ± 0.7	46.0	70.2 ± 0.7	$+24.2 \pm 0.7$
Cs-137	661.7	665.3 ± 3.3	477.3	478.2 ± 3.2	$+0.9 \pm 3.2$
Mn-54	834.8	841.1 ± 4.2	639.22	648.4 ± 3.7	$+9.2 \pm 3.7$
Zn-65	1115.5	1140.0 ± 5.7	907.62	860.7 ± 4.8	-46.9 ± 4.8
KCl	1460.8	1501.2 ± 7.5	1243.0	1216.1 ± 6.2	-26.9 ± 6.2

is what we expect and is an interesting merger of information theory and nuclear physics, which shows how the increasing photon energy with nuclides can lead to more disordered states.

4.3 Conclusion

The goals of this experiment were to experimentally verify the relativistic relationship between energy and momentum for high-speed electrons produced through Compton scattering, and to analyze the information content of detected γ-ray spectra. Using an SRD coupled to a photomultiplier tube, we obtained spectra for several γ-emitting sources and determined both the photopeak and Compton edge energies through energy calibration of the MCA and MCB systems. Our determination of the Compton edges shown in table 3 shows very good agreement with known values such as from the IAEA database [4], with the largest residuals being due to detector response or low count rate samples.

From this, we calculated the recoil electron momenta and compared our data to both the classical and relativistic energy–momentum relations. The measured results showed near-perfect agreement with the relativistic prediction

$$E^2 = p^2c^2 + m_e^2c^4,$$

while the classical model $K = p^2/2m_e$ significantly deviated at high energies. We quantify this by showing that relatavistic residuals are on the order 10^{-32} while classical residuals are on the order 1 when predicting the electron rest energy.

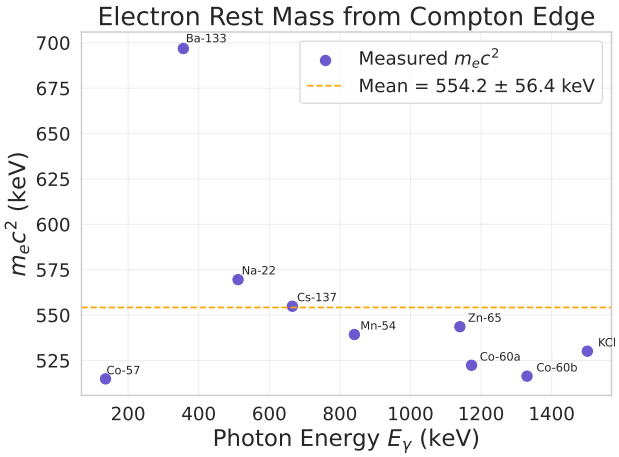

Figure 10: Electron energy calculated as a function of Compton edges and photopeak values for measured γ-emission spectra. This was determined using equation 6.

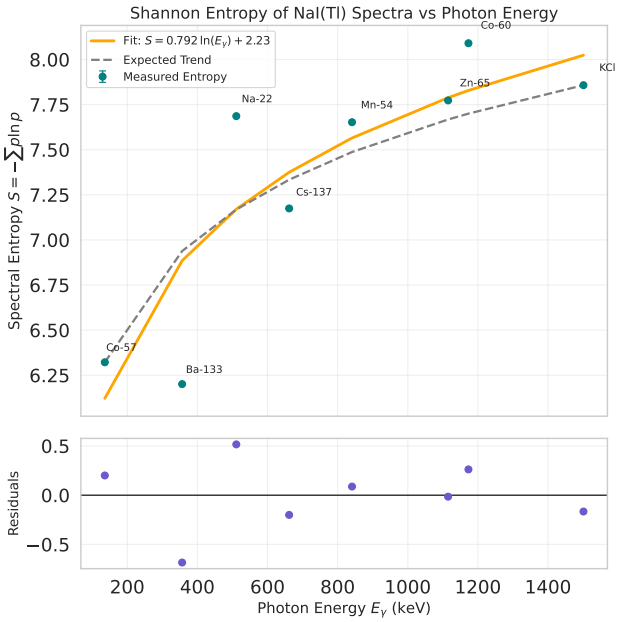

Figure 11: Measured Shannon entropy of gathered spectra as a function of photon energy. The orange line shows the best-fit trend, while the dashed line represents the expected theoretical dependence $S \propto \ln(E_\gamma)$.

Additionally, an unknown γ-emitter was successfully identified as Cs-137 based on its characteristic 662 keV photopeak and 478 keV Compton edge, confirming the reliability of our calibration and analysis methods.

We also experimentally determined electron rest energy was found to be $m_ec^2 = 554.2 \pm 56.4$ keV, consistent with the accepted value of 511 keV within uncertainty.

Finally, a Shannon entropy analysis was performed on the spectral complexity of each isotope's γ-spectrum, and gave a logarithmic dependence on photon energy,

$$S = (0.792 \pm 0.03)\ln(E_\gamma) + (2.23 \pm 0.05),$$

which shows the increased distribution of photon energies from Compton scattering at higher E_γ. These results confirm the validity of relativistic dynamics and demonstrate how measures such as entropy can be applied to radiation spectra to characterize their physical complexity.

This experiment shows a landmark result in the realm of physics, that objects moving close to the speed of light have very different and classically unpredicted properties. This serves as confirmation of relativity, one of the most important and elegant concepts in physics. Not only has this experiment shown to confirm the theory of electricity, it has been a valuable exercise in independent laboratory procedure.

4.4 Future Work Considerations

Future versions of this experiment could benefit from extended data collection periods and the use of higher-resolution SRDs. Varying parameters for signal processing paremters such as the preamplifier capacitance and the amplifier gain could also prove to be valuable. In addition, future work could expand the entropy analysis to compare different detector materials or examine temporal noise characteristics in photon statistics.

Acknowledgements: Thank you to my partner, Adin Viera, and to the lab TAs, Joshua and Oorie.

References

[1] Arthur H. Compton. "A Quantum Theory of the Scattering of X-rays by Light Elements". In: *Physical Review* 21.5 (1923), pp. 483–502. DOI: 10.1103/PhysRev.21.483.

[2] Mark G. Dowsett, Nancy Roberts, and Robert Campbell. "Practical Considerations for Gamma Ray Spectroscopy with NaI(Tl)". In: *Radiation Measurements* 121 (2019), pp. 1–9. DOI: 10.1016/j.radmeas.2018.11.003.

[3] Albert Einstein. "Ist die Trägheit eines Körpers von seinem Energieinhalt abhängig?" In: *Annalen der Physik* 18 (1905). English translation: "Does the Inertia of a Body Depend upon Its Energy Content?", pp. 639–641. DOI: 10.1002/andp.19053231314.

[4] International Atomic Energy Agency. *Gamma-ray energies and emission probabilities ordered by radionuclide (Standard dataset)*. Accessed 27 October 2025. 2023.

[5] Glenn F. Knoll. *Radiation Detection and Measurement*. 4th. Hoboken, NJ: John Wiley & Sons, 2010. ISBN: 9780470131480.

[6] Idaho National Laboratory. *NaI(Tl) Spectrum Catalogue – Table of Photopeak Data*. Technical Report Revision 1. Includes full-energy photopeak data for NaI(Tl) detectors. Idaho National Laboratory, 2020. URL: https://gammaray.inl.gov/Shared%20Documents/naicat.pdf.

[7] Xin Li, Ming Zhao, and Song Wang. "An Overview of the Compton Scattering Calculation". In: *Crystals* 11.5 (2021), p. 525. DOI: 10.3390/cryst11050525. URL: https://www.mdpi.com/2073-4352/11/5/525.

[8] Monash University. *Relativistic vs Classical Momentum Graph*. https://www.monash.edu/student-academic-success/physics/relativity/mass-energy-theorem. From the Monash University Student Academic Success Physics Resources, section on Relativity and the Mass–Energy Theorem. Accessed October 2025. 2025.

[9] Openstax. *8.1 Linear Momentum, Force, and Impulse*. Rice University. URL: https://openstax.org/books/physics/pages/8-1-linear-momentum-force-and-impulse.

[10] Ortec. "905 Series NaI(Tl) Scintillation Radiation Detectors". In: (). URL: https://www.ortec-online.com/products/radiation-detectors/scintillation-radiation-detectors/scintillation-detector-types/905-series.

[11] Ortec. "Aspec-927 Dual Multichannel Buffer". In: (). URL: https://www.ortec-online.com/-/media/ametekortec/manuals/9/927-mnl.pdf?la=en&revision=daf2a438-c355-4df8-91b9-23907cf6efab.

[12] Ortec. "Gamma-Ray Spectroscopy Using NaI(Tl)". In: (). URL: https://www.ortec-online.com/-/media/ametekortec/third%20edition%20experiments/3-gamma-ray-spectroscopy-using-nai-tl.pdf?utm_source=chatgpt.com.

[13] Ortec. "Introduction to Amplifiers". In: (). URL: https://www.ortec-online.com/-/media/ametekortec/other/amplifier-introduction.pdf.

[14] Ortec. *Preamplifier Introduction*. URL: https://www.ortec-online.com/-/media/ametekortec/other/preamplifier-introduction.pdf?la=en.

[15] Ortec. "Simply Managing Dead Time Errors in Gamma-Ray Spectrometry". In: (). URL: https://www.ortec-online.com/-/media/ametekortec/application%20notes/an63.pdf?la=en&.

[16] Libretexts Physics. "6.4: The Compton Effect". In: (). URL: https://phys.libretexts.org/Bookshelves/University_Physics/University_Physics_(OpenStax)/University_Physics_III_-_Optics_and_Modern_Physics_(OpenStax)/06%3A_Photons_and_Matter_Waves/6.04%3A_The_Compton_Effect.

[17] ScienceDirect Topics. *Scintillation Detector*. https://www.sciencedirect.com/topics/engineering/scintillation-detector. Overview and diagram of scintillation detectors and photomultiplier operation. Accessed October 2025. 2025.

[18] Claude E. Shannon. "A Mathematical Theory of Communication". In: *Bell System Technical Journal* 27.3 (July 1948), pp. 379–423. DOI: 10.1002/j.1538-7305.1948.tb01338.x. URL: https://people.math.harvard.edu/~ctm/home/text/others/shannon/entropy/entropy.pdf.